Energy Conversion and Management 108 (2016) 355–365

Contents lists available at ScienceDirect

Energy Conversion and Management

journal homepage: www.elsevier.com/locate/enconman

A simple maximum power point tracker for thermoelectric generators

Alexandros Paraskevas, Eftichios Koutroulis *

School of Electronic and Computer Engineering, Technical University of Crete, Chania GR-73100, Greece

ARTICLE INFO

Article history:
Received 7 July 2015
Accepted 10 November 2015
Available online 7 December 2015

Keywords:
Thermoelectric generator
Maximum Power Point Tracking
Boost converter
Energy harvesting

ABSTRACT

ThermoElectric Generators (TEGs) are capable to harvest the ambient thermal energy for power-supplying sensors, actuators, biomedical devices etc. in the μW up to several hundreds of Watts range. In this paper, a Maximum Power Point Tracking (MPPT) method for TEG elements is proposed, which is based on controlling a power converter such that it operates on a pre-programmed locus of operating points close to the MPPs of the power–voltage curves of the TEG power source. Compared to the past-proposed MPPT methods for TEGs, the technique presented in this paper has the advantage of operational and design simplicity. Thus, its implementation using off-the-shelf microelectronic components with low-power consumption characteristics is enabled, without being required to employ specialized integrated circuits or signal processing units of high development cost. Experimental results are presented, which demonstrate that for MPP power levels of the TEG source in the range of 1–17 mW, the average deviation of the power produced by the proposed system from the MPP power of the TEG source is 1.87%.

1. Introduction

The application of energy harvesting technologies has emerged during the last years for satisfying the power-supply requirements of power-autonomous devices, by scavenging the mechanical, waste heat, biological etc. energy, which is available in their surrounding environment [1]. The harvested energy is then interfaced to a microelectronic energy management system for conversion to a form suitable for power-supplying the target electronic load. Among the energy harvesting alternatives, the ThermoElectric Generators (TEGs) comprise multiple semiconductor thermocouples (e.g. constructed using Bismuth Telluride with *p*- and *n*-doping), which are capable to generate electric energy when subject to a temperature difference across their hot and cold sides [2]. The TEGs feature high reliability, do not contain moving parts [3] and exhibit compactness, long-lifetime and low-weight features. Thus, they are suitable for installation on surfaces where thermal flows are developed (e.g. human body, pipes of hot liquids, combustion engines, vehicle exhausts etc.). The TEG devices are capable to power supply, in the μW up to several hundreds of Watts range, medical devices, wearable and wireless sensors, remote actuators, interplanetary space flight systems etc. (e.g. [4–8]).

A generalized block diagram of a thermoelectric energy harvesting system is illustrated in Fig. 1(a). The TEG power source is connected to a DC/DC power converter, which interfaces the generated power to the system load or an energy storage unit (rechargeable battery or super-capacitor) [9]. An example of the power–voltage characteristic of a TEG module is depicted in Fig. 1(b), indicating that the TEG power source exhibits a point where the generated power is maximized (i.e. Maximum Power Point, MPP). The necessary condition that must be satisfied by a Maximum Power Point Tracking (MPPT) process for maximizing the power generated by the TEG source, is the following:

$$\frac{\partial P_{TEG}}{\partial V_{TEG}} = 0 \tag{1}$$

where P_{TEG} (W), V_{TEG} (V) is the TEG output power and voltage, respectively.

A wide variety of techniques have been proposed in the past for performing the MPPT process in TEG-based energy harvesting systems, as analyzed in the following.

The Perturbation and Observation (P&O) or hill-climbing MPPT technique is based on the result of comparison of successive measurements of the TEG output power [10,11], which are performed before and after, respectively, the duty cycle of the power converter has been perturbed. The Incremental-Conductance (InC) algorithm is based on the principle that at the MPP of the TEG generator, it holds that [11]:

* Corresponding author. Tel.: +30 28210 37233; fax: +30 28210 37542.
E-mail address: efkout@electronics.tuc.gr (E. Koutroulis).

http://dx.doi.org/10.1016/j.enconman.2015.11.027
0196-8904/

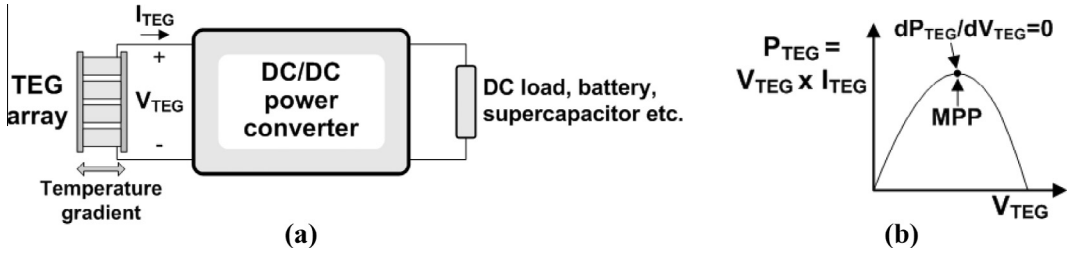

Fig. 1. A thermoelectric energy harvesting system: (a) a generalized block diagram and (b) an example of the power–voltage characteristic of a TEG module.

$$\frac{\partial P_{TEG}}{\partial V_{TEG}} = 0 \Rightarrow \frac{\partial (I_{TEG} \cdot V_{TEG})}{\partial V_{TEG}} = I_{TEG} + \frac{\partial I_{TEG}}{\partial V_{TEG}} V_{TEG} = 0 \Rightarrow \frac{\partial I_{TEG}}{\partial V_{TEG}} = -\frac{I_{TEG}}{V_{TEG}} \quad (2)$$

where I_{TEG} (A) is the TEG output current.

Thus, by measuring and comparing the values on the two sides of (2), the TEG operating point is progressively moved to the MPP. A voltage-trend detection circuit has been designed in [12], where the gradient of a Boost-converter output power is detected by measuring the corresponding output voltage, thus achieving a low-power implementation of the hill-climbing MPPT approach. The MPPT efficiency of the P&O and InC algorithms is affected by circuit noise, as well as by the accuracy of calculating the TEG output power or current gradient. As discussed in [11], increasing the perturbation step results in a high steady-state oscillation around the MPP, which reduces the TEG power production. On the other hand, increasing the accuracy of the power or gradient measurements, increases the complexity and power consumption of the MPPT control unit. This operational characteristic is especially crucial in low-power TEG applications where the power production of the TEG source and the power consumption of the control-unit are of the same order of magnitude.

For performing the MPPT process in [13,14], the TEG power source is periodically disconnected from the power converter in order to measure its open-circuit voltage, $V_{TEG,oc} = V_{TEG}|_{I_{TEG}=0}$. Then, SEPIC- and Boost-type DC/DC power converters, respectively, are controlled such that the TEG source operates at $V_{TEG,oc}/2$, which corresponds to the MPP. This technique is usually referred to as the "fractional open-circuit voltage" (FOCV) MPPT method. Similarly, in the "fractional short-circuit current" (FSCC) MPPT method, the TEG source is periodically set to operate under a short-circuit condition and the corresponding short-circuit output current, $I_{TEG,sc}$, is measured (i.e. $I_{TEG,sc} = I_{TEG}|_{V_{TEG}=0}$) [11,15]. The power stage is then controlled such that the TEG output current is equal to the half of the previously measured short-circuit TEG current, thus achieving operation at the MPP. Despite their operational simplicity, the FOCV and FSCC MPPT methods are not able to track the short-term changes of the MPP, which occur between successive measurements of the open-circuit voltage or short-circuit current. Else, the sampling frequency of the open-circuit voltage or short-circuit current should be substantially increased, resulting in power loss, since the power production of the TEG device is suspended during the open-circuit voltage or short-circuit current measurements. In order to avoid interrupting the TEG source operation for measuring the open-circuit voltage, the FOCV technique has been implemented in [1] by employing a pair of temperature sensors for measuring the temperature gradient developed across the hot and cold sides, respectively, of the TEG source and estimating the corresponding open-circuit voltage of the TEG source. However, this approach has the disadvantage that the temperature sensors employed increase the cost of the MPPT system, especially in the case that the operating temperature range of the TEG source is high (e.g. in combustion engine applications).

A single-sensor MPPT approach for TEGs is proposed in [16]. The inductor current of a Boost-type DC/DC power converter is measured and used to estimate the MPP of the TEG power source by using a model of the power converter according to the state-space averaging technique. In order to apply this method, a Digital Signal Processing (DSP) unit must be employed for performing the calculations dictated by the power converter model during the MPPT process.

In another class of TEG MPPT techniques, the internal resistance of TEGs is considered approximately constant over the entire span of operating temperature gradients [17]. Based on this operating principle, the input impedance of a Boost-type DC/DC converter operating in the discontinuous-conduction mode, R_{in}, is tuned in [17] to match the TEG series-resistance [i.e. "Impedance Matching" (ImpM) MPPT method], such that the TEG source always operates at the MPP. The input impedance tuning is implemented by selecting the switching frequency, f_s and ON-time, t_1, of the converter power switch, given the value of the power converter inductance, L, as follows:

$$R_{in} = \frac{2 \cdot L}{t_1^2 \cdot f_s} \quad (3)$$

A similar approach has also been employed in [18]. The ImpM method has the following disadvantages: (i) the efficiency of the MPPT process is affected by the accuracy of setting the inductance, incorporated in the power converter, to the desired value (due to inductance value tolerance, as well as its variation with the operating temperature), (ii) it does not enable tuning the inductance and switching frequency to the appropriate values, which would optimize the power converter performance in terms of metrics such as the power conversion efficiency and cost and (iii) the power converter operation in the discontinuous-conduction mode is not desirable at higher power levels, since power semiconductors of a high current rating would be required in that case.

The Extremum Seeking Control (ESC) MPPT technique, which is proposed in [19], is based on the implementation of a feedback control loop, where a sinusoidal perturbation is applied to the duty cycle of the DC/DC converter control signal, resulting in a perturbation of the TEG-generated power. Then, the output power of the TEG source is measured and the resulting signal is demodulated, indicating the gradient of the TEG power–voltage curve at the corresponding operating point. This information is used to derive the new duty-cycle perturbation, which will force the TEG operating point to move toward the MPP of the TEG source, where condition (1) holds. The disadvantage of the ESC MPPT method is that in order to operate successfully, the values of multiple parameters of the control loop must be properly adjusted.

In this paper, an alternative MPPT method for TEG devices is proposed, which is based on controlling a power converter such that it operates on a preprogrammed locus of operating points, which reside close to the MPPs of the power–voltage curves of

the TEG power source. Compared to the past-proposed MPPT methods described above, the technique presented in this paper has the advantage of offering more operational and design simplicity. These features enable to avoid the use of specialized signal-processing and control units and implement the TEG MPPT system using low-cost and off-the-shelf microelectronic components, thus reducing the development cost of the overall MPPT system. Therefore, a universal MPPT method for TEGs is proposed in this paper, which is suitable for application in both low-power energy harvesting applications, where it is crucial to reduce the power consumption of the MPPT control unit, as well as high-power TEG-based energy production systems.

This paper is organized as follows: the modeling and operational characteristics of TEG devices are described in Section 2; the proposed MPPT system is presented in Section 3 and the experimental results are presented in Section 4; a comparison of the hardware requirements for implementing the proposed and prior-art MPPT methods is presented in Section 5 and, finally, the conclusions are discussed.

2. Modeling and operational characteristics of TEGs

A TEG device consists of multiple thermocouple elements that are connected electrically in series and thermally in parallel [20]. The basic structure of a thermocouple element is presented in Fig. 2(a) [21]. The TEG structure consists of two heavily doped semiconductors with their edges connected to conductors, thus creating an electrical loop. During operation, different temperatures are applied on these junctions [i.e. T_H and T_C in Fig. 2(a)] causing electrons and holes in the n-type and p-type semiconductors, respectively, to flow from the hot to the cold side. This process results in the development of an electric field across the p and n semiconductors, due to the Seebeck effect. The voltage $V_{TEG,oc}$ (V), which is produced at the cold junction of Fig. 2(a) under open-circuit conditions (i.e. in case that the thermoelectric element load resistance is $R_L = \infty$), is proportional to the temperature difference between the hot and cold junctions, ΔT (°C), according to the following equation [21]:

$$V_{TEG,oc} = V_{TEG}|_{I_{TEG}=0} = \alpha_{pn} \cdot (T_H - T_C) = \alpha_{pn} \cdot \Delta T \quad (4)$$

where α_{pn} (V/°C) is the Seebeck coefficient between the p and n semiconductors and T_H (°C), T_C (°C) are the temperatures of the hot and cold side, respectively.

The p and n semiconductors have positive and negative Seebeck coefficients, respectively. Thus, parameter α_{pn} is positive. The values of T_H and T_C in (4) are calculated as analyzed in [21], taking into account: (i) the Joule effect and (ii) the heat transfer rates from the thermal source to the hot junction through the top ceramic plate and from the cold junction to the environment through the bottom ceramic plate [as shown in Fig. 2(a)] due to the thermal conductance of the ceramic plates.

The equivalent circuit of a TEG element is depicted in Fig. 2(b). Assuming that a load, R_L, is connected to the terminals of the thermoelectric element, then the output power of the thermoelectric generator is calculated using (4), as follows:

$$P_{TEG} = \frac{\left(V_{TEG,oc} \cdot \frac{R_L}{R_{TEG}+R_L}\right)^2}{R_L} = \frac{\alpha_{pn}^2 \Delta T^2 R_L}{(R_{TEG}+R_L)^2} \quad (5)$$

where R_{TEG} (Ω) is the internal electric resistance of the thermoelectric element.

Using ceramic plates with a high thermal conductance enables the development of a temperature gradient across the outside surfaces of the TEG element [i.e. ΔT_o in Fig. 2(a)], which is close to ΔT, thus maximizing the power production of the thermoelectric energy conversion device.

The maximum power transfer from the TEG source to the load is achieved under the condition that $R_{TEG} = R_L$. In this case, the power transferred to the load is calculated using the following equation:

$$P_{TEG,\max} = \frac{\alpha_{pn}^2 \Delta T^2}{4R_{TEG}} \quad (6)$$

To further explore the operational characteristics of thermoelectric generators, a TEG device with $\alpha_{pn} = 0.026$ V/°C, $V_{TEG,oc} = 0.63$ V, $I_{TEG,sc} = 0.02$ A and $P_{TEG,\max} = 3.19$ mW for $\Delta T = 25$ °C, has been considered. A software program operating under the MATLAB platform has been developed, which calculates the current–voltage and power–voltage characteristics of the TEG element based on the modeling of TEG devices presented above. Examples of the theoretically calculated current–voltage and power–voltage characteristics of the TEG device under consideration for various values of ΔT, are depicted in Fig. 3(a) and (b). The corresponding values of T_H and T_C are shown in Fig. 3(c) and (d), respectively. It is observed that for each value of ΔT, a unique MPP is exhibited by the corresponding power–voltage characteristic of the TEG source. Due to the linearity of the TEG element equivalent circuit, consisting of a voltage source connected in series with a resistance [Fig. 2(b)], an array formed by multiple such TEG elements connected in series and parallel is also modeled by an equivalent circuit of the same form. Thus, such a TEG array exhibits a power–voltage curve with a single MPP for each value of ΔT, without any local MPPs. This has also been verified through the experimental results, which will be presented in the following.

The modeling and operational characteristics of TEGs, which have been presented above, have been exploited for the development of a new MPPT method for TEG devices, as analyzed next.

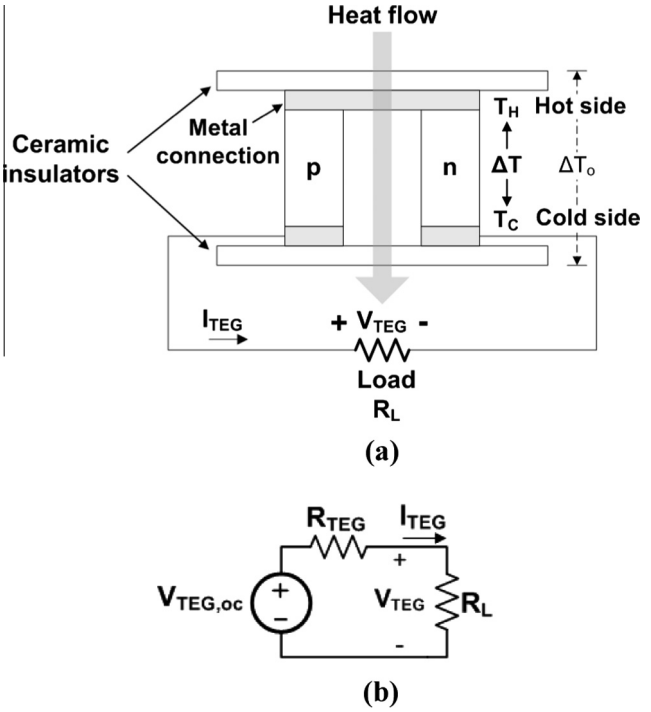

Fig. 2. A TEG element: (a) structure and (b) equivalent circuit.

3. The proposed MPPT system

According to the equivalent circuit of the TEG element, which is illustrated in Fig. 2(b), for each value of the temperature gradient ΔT it holds that:

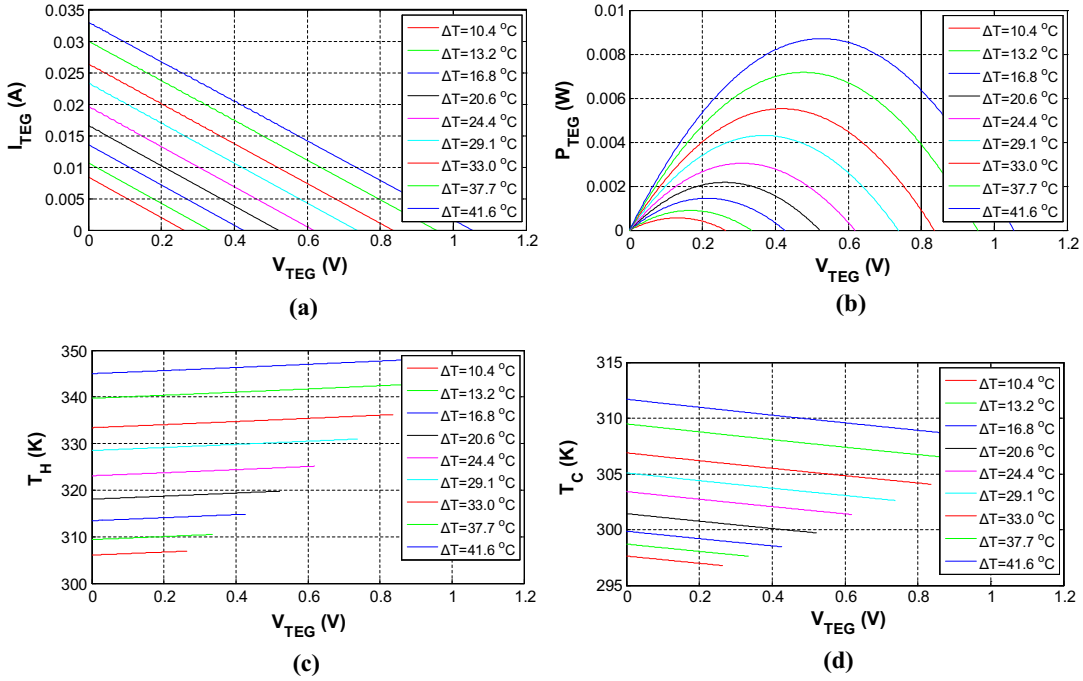

Fig. 3. The theoretically calculated characteristics of a TEG device for various values of ΔT: (a) current–voltage, (b) power–voltage, (c) hot junction temperature–voltage and (d) cold junction temperature–voltage.

$$V_{TEG} = V_{TEG,oc} - I_{TEG} \cdot R_{TEG} \Rightarrow \frac{\partial I_{TEG}}{\partial V_{TEG}} = -\frac{1}{R_{TEG}} \tag{7}$$

In low-power energy harvesting applications, the power consumption of the MPPT control unit may become comparable to the power generated by the power source. Thus, it is indispensable to optimally explore the trade-off between increasing the accuracy of the MPPT system and reducing the power consumption of the microelectronic subsystem, which executes the MPPT control operation. In order to simplify the implementation of the MPPT control system and reduce its power consumption, in the proposed MPPT method the variation of R_{TEG} with temperature (which is also a function of the TEG output current due to the Joule effect [21]) is assumed negligible, as also considered in [17,18]. In such a case, the value of R_{TEG} remains constant to $R_{TEG} = R_{TEG,c}$ for all values of ΔT, where $R_{TEG,c}$ is the constant value of the TEG resistance. Thus, considering (7), in the proposed MPPT method the value of $-\frac{I_{TEG}}{V_{TEG}}$ in (2) is compared with $-\frac{1}{R_{TEG,c}}$ instead of $\frac{\partial I_{TEG}}{\partial V_{TEG}}$, which is used in the InC method and the condition for convergence to the TEG source MPP under any temperature gradient conditions is the following:

$$I_{TEG} - \frac{1}{R_{TEG,c}} V_{TEG} = 0 \tag{8}$$

The actual resistance of the TEG source deviates from the (constant) value of the TEG resistance, which is considered in (8), due to the temperature sensitivity of the TEG resistance, the tolerance with respect to the datasheet value etc. The output power of the TEG source, which results for each value of ΔT when operating at the operating points defined by (8), $P_{TEG,o}$, is calculated by setting $R_L = R_{TEG,c}$ in (5), as follows:

$$P_{TEG,o} = \frac{\alpha_{pn}^2 \Delta T^2 R_{TEG,c}}{(R_{TEG} + R_{TEG,c})^2} \tag{9}$$

where R_{TEG} is the actual resistance of the TEG source for each value of ΔT.

For commercially available TEG devices, the value of R_{TEG} changes by approximately 0.3—0.75% per 1 °C increase of the average temperature between the hot and cold sides. Additionally, a 12% maximum drift of R_{TEG} with the temperature gradient ΔT has been reported in [14]. In these cases, by setting $R_{TEG,c}$ equal to the value of R_{TEG} at the middle of the temperature-gradient range, the resulting deviation of $P_{TEG,o}$ from the corresponding MPP power of the TEG source, $P_{TEG,\max}$, which is given by (6), is less than 0.41% for temperature gradients in the range of $\Delta T = 1$—40 °C. This deviation is increased to 1.1% for $\Delta T = 1$—100 °C. Thus, by following the TEG source operating points defined by (8), without considering the effect of temperature on the TEG resistance value, the resulting deviation of the generated power from the actual MPP power remains at an acceptable level and, simultaneously, the hardware complexity and power consumption of the MPPT controller are reduced. For avoiding the MPPT accuracy degradation due to deviation of the actual value of R_{TEG} with respect to the information provided in the manufacturer datasheet, the value of $R_{TEG,c}$ applied in (8) may be derived experimentally. This process may be implemented by applying a characterization process of the TEG device to be employed in the target application, as described in [21]. The drift of R_{TEG} due to aging may be compensated by applying such a characterization process periodically and then re-tuning the proposed MPPT system [through (8)] to operate with the new value of $R_{TEG,c}$.

A block diagram of the power conversion system, which implements the proposed MPPT method described above, is depicted in Fig. 4(a). The topology of the power-processing circuit (i.e. Buck, Boost, Buck-Boost etc.) is selected according to the magnitudes of the DC input and output voltages [22]. The proposed MPPT system has been designed to operate with TEG input power sources which generate a low DC output voltage. Thus, a Boost-type DC/DC power converter is employed to interface the TEG-generated power to a battery bank. The Boost-type DC/DC converter may be configured by the designer to operate either in the Continuous-Conduction Mode (CCM), or in the Discontinuous-Conduction Mode (DCM) [22]. In the former case, the input and output voltage levels, V_{in}

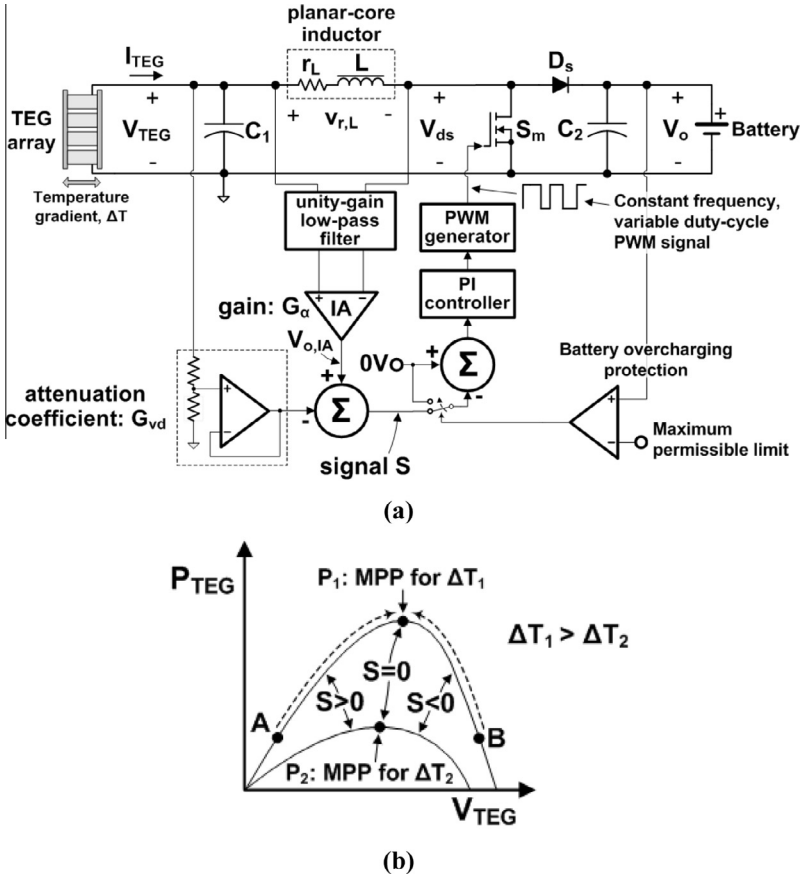

Fig. 4. The proposed MPPT system: (a) block diagram and (b) the MPPT tracking process.

(V) and V_o (V), respectively, are related according to the following equation:

$$V_o = \frac{1}{1-D} \cdot V_{in} \tag{10}$$

where D is the duty cycle of the power-switch control signal and $0 \leqslant D \leqslant 1$.

For operation in DCM, a lower value of inductance L may be employed in the Boost-type DC/DC converter. This results in an increase of the power conversion efficiency and a reduction of the inductor cost, but the resulting peak currents of the power MOSFET and diode [i.e. S_m and D_s, respectively, in Fig. 4(a)] are higher than in CCM. The power MOSFET type is selected such that the conduction and switching power losses during the MPPT operation remain at an acceptable level. Also, a Schottky diode is used for obtaining a low voltage drop across the diode, as well as a fast recovery time. The capacitors C_1 and C_2 in Fig. 4(a) are used for eliminating the ripple of the TEG source output current and DC/DC converter output voltage, respectively.

The current flowing through the input inductor of the Boost-converter consists of an AC ripple imposed on a DC component [22], which is equal to the DC current generated by the TEG source [i.e. I_{TEG} in Fig. 4(a)]. The average values of the AC current ripple of the converter input current and voltage developed across L are equal to zero under steady-state conditions [22]. Thus, as shown in Fig. 4(a), in the proposed control unit the TEG output current, I_{TEG}, is calculated by passing the voltage $v_{r,L}$ through an RC low-pass filter with a 3-dB cut-off frequency, which has been set equal to 1% of the Boost-converter switching frequency. The generated signal is proportional to I_{TEG} and it is amplified by connecting it to the AD8236 micro-power instrumentation amplifier [i.e. IA in Fig. 4(a)], in order to obtain a high common-mode rejection ratio. Thus, the TEG current is measured with an overall gain, G_{id}, which depends on the series resistance of the power inductor, r_L (Ω) and the IA gain, G_a, as follows:

$$G_{id} = \frac{V_{o,IA}}{I_{TEG}} = r_L \cdot G_a \tag{11}$$

where $V_{o,IA}$ (V) is the IA output voltage.

The TEG output voltage is measured using a resistive voltage divider with an attenuation coefficient equal to G_{vd}, which is connected to an operational-amplifier-based voltage-follower. The measured current and voltage signals are then added, resulting in the production of the following signal:

$$S = G_{id} \cdot I_{TEG} - G_{vd} \cdot V_{TEG} = G_{id} \cdot \left(I_{TEG} - \frac{G_{vd}}{G_{id}} \cdot V_{TEG} \right) \tag{12}$$

In order to perform the MPPT process in the proposed technique, the value of $\frac{G_{vd}}{G_{id}}$ in (12) is set to a constant value, which is equal to $\frac{1}{R_{TEG,c}}$, thus implementing (8). As described above, the series resistance of the TEG power source, R_{TEG}, is either derived by the datasheet information provided by its manufacturer or it may be measured experimentally for achieving a higher accuracy. As shown in Fig. 4(b), the value of S in (12), is positive on the left side of the TEG power–voltage characteristic, negative on its right side and zero at the TEG MPP. According to Fig. 4(a), in the proposed MPPT system the signal S is compared with 0 V and the resulting error is interfaced to a PI-controller, which then drives a Pulse Width Modulation (PWM) generator for producing the variable duty-cycle/constant-frequency control signal of the Boost-type DC/DC converter power MOSFET. During operation, the value of S in (12)

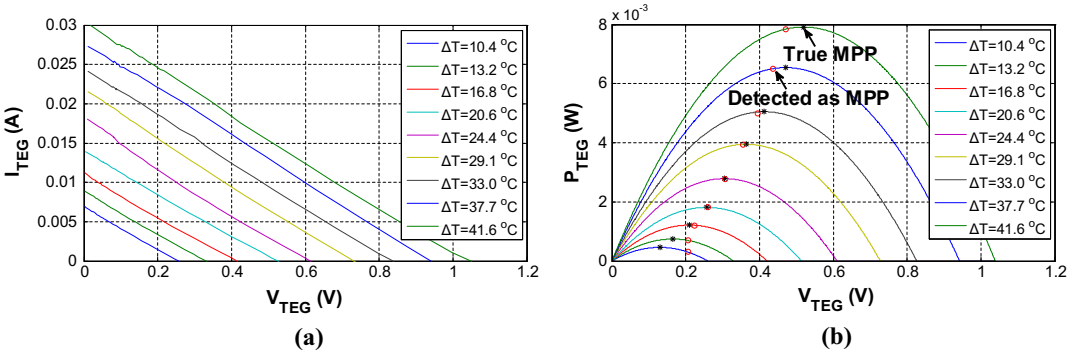

Fig. 5. Experimental characteristics for one TEG device: (a) current–voltage and (b) power–voltage.

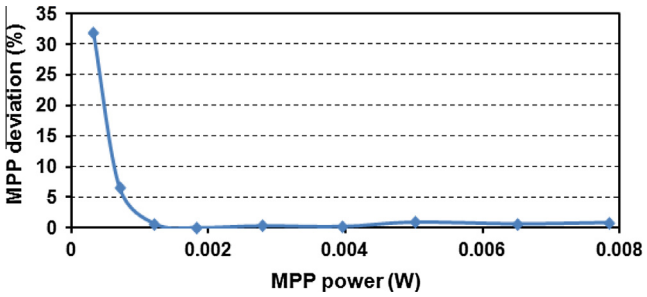

Fig. 6. The power deviation between the actual MPPs of the TEG power–voltage curve and the operating points detected as MPPs by the proposed system for various values of ΔT.

is progressively reduced to zero. Thus, irrespectively of the initial operating point [i.e. point A or B in Fig. 4(b)], the proposed process is capable to ensure convergence close to the corresponding MPP for any temperature gradient developed across the surfaces of the TEG source [e.g. P_1 and P_2 in Fig. 4(b)].

In order to avoid battery damage due to overcharging, a protection circuit has been designed and implemented. As shown in Fig. 4(a), when the battery bank has been charged to the desirable level, then the overcharge protection system connects the inverting input of the adder to 0 V. As a consequence, the PWM signal is set to zero and the Boost converter operation is suspended. The control unit is power-supplied by the battery bank, which is connected at the output of the DC/DC converter. Alternatively, a super-capacitor may also be used for storing the TEG-generated energy. In the proposed system it has been assumed that when the operation of the MPPT system must be initiated, the charge existing in the output energy-storage device (i.e. battery or super-capacitor) is adequate to ignite the operation of the MPPT control unit. In TEG applications where this condition does not apply, then start-up mechanisms such as those presented in [18,23] for thermoelectric energy harvesting systems, may also be incorporated in the proposed MPPT system in order to provide the initial energy required by the MPPT control unit to start operating. However, since this study is focused on the design and operation of the TEG MPPT system, this issue was not further investigated.

4. Experimental results and discussion

An experimental prototype of the proposed system has been constructed for evaluating its performance for various TEG configurations and operating conditions. The Nextreme eTEG HV56 thermoelectric generators have been employed as energy sources, while the proposed MPPT system has been built using discrete parts of commercially-available, low-voltage and low-power integrated circuits. Two Ni–MH batteries connected in series with a total nominal voltage of $V_o = 2.4$ V have been connected at the output terminals of the Boost-type DC/DC converter shown in Fig. 4(a). The Boost converter constructed, comprises a 28 μH inductor with a series resistance of $r_L = 5.55$ mΩ, a BAT60A Schottky diode and a Sir802dp power MOSFET, which correspond to components L, D_s and S_m, respectively, in Fig. 4(a). The input and output filter capacitors of the Boost converter were set at $C_1 = 470$ μF and $C_2 = 1000$ μF, respectively. A planar core has been employed in the power inductor of the Boost-type power converter [i.e. L in Fig. 4(a)] for reducing the size of the power processing subsystem. After performing calculations for various planar-core types and switching frequency values, the R-41805 EC-type ferrite planar core, as well as a switching frequency of 100 kHz, have been selected for minimizing the power loss of the inductor. The voltage-follower, adder and PI-controller, which are depicted in Fig. 4(a), have been built using the LMP2234 micro-power

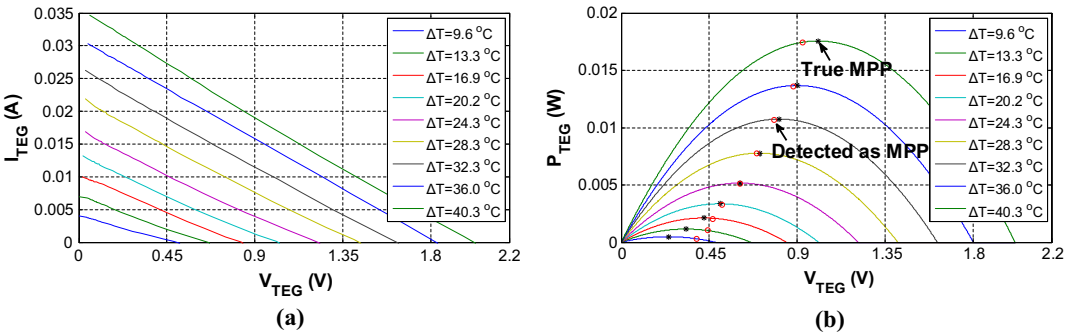

Fig. 7. Experimental characteristics for two TEG modules connected in series: (a) current–voltage and (b) power–voltage.

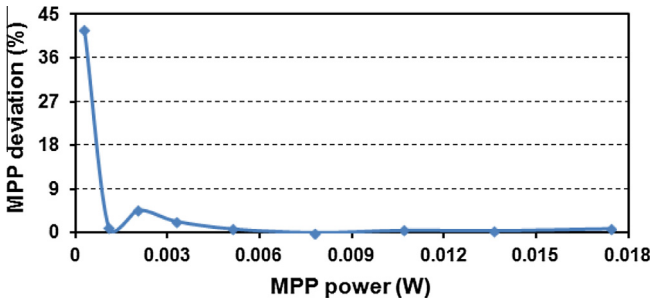

Fig. 8. The percentage deviation between the actual MPPs of the power–voltage curve of a TEG array consisting of two TEG modules connected in series and the MPPs detected by the proposed system as MPPs, for various values of ΔT.

precision operational amplifier. The PWM generator, comprising a comparator and a triangular wave generator, is based on the AD8515 low-power operational amplifier. However, alternative types of components may also be employed by the designer for implementing the proposed MPPT system, such that specific requirements of the target application are satisfied (e.g. in terms of power rating, output voltage level etc.).

The experimental current–voltage curves of one TEG device for temperature gradients in the range of 10.4–41.6 °C, which are developed in heat harvesting applications on aircrafts, hot liquids, human body etc. [5,16,24], are illustrated in Fig. 5(a). These current–voltage curves have been measured by disabling the operation of the MPPT control unit and iteratively modifying the DC/DC Boost converter duty cycle over the 0–100% range with a 3% step through an external square-wave generator. Due to non-linear operation exhibited by the control system [Fig. 4(a)] at low input voltage levels, small amplitude ripples are observed in Fig. 5(a) in the region between 0.08 V and 0.1 V, where the duty cycle value is close to 80%. The corresponding experimental power–voltage curves are depicted in Fig. 5(b). The operating points detected experimentally as MPPs by the proposed MPPT system and the corresponding actual MPPs of the power–voltage curves are also depicted in that figure. In order to perform the MPPT process, the control unit was then configured such that it operates with a value of $R_{TEG,c} = 25.7\ \Omega$ in (8). This value is equal to the experimentally measured internal resistance of the TEG device at $\Delta T = 0$ °C. Next, the tracking accuracy of the proposed system at various temperature levels has been evaluated. The percentage deviation between the actual MPPs exhibited by the TEG power–voltage curve at various values of temperature gradient, ΔT, in the range of 10.4–41.6 °C and the corresponding operating points detected as MPPs by the proposed system, is plotted in Fig. 6. The power deviation is 0.03–0.95%, while it increases up to 31.99% for ΔT values less than 13.2 °C. This power deviation is 0.01–1.86% of the MPP power produced for ΔT = 41.6 °C.

The experimental current–voltage curves of two TEG modules connected in series, for several temperature gradients, are shown in Fig. 7(a). In this case, the proposed system has been configured to operate with a value of $R_{TEG,c} = 2 \times 25.7 = 51.4\ \Omega$ in (8). The experimentally measured power–voltage curves of two TEG devices connected in series are shown in Fig. 7(b). The operating points derived experimentally as MPPs by the proposed MPPT system and the corresponding actual MPPs for each value of the temperature gradient, ΔT, are also displayed in that figure. The resulting variation of the tracking accuracy with operating temperature is illustrated in Fig. 8. It is observed that for MPPs corresponding to ΔT values in the range of 13.3–40.3 °C, the MPPs detected by the proposed system deviate by the corresponding actual MPPs of the TEG input source by 0.02–4.69%. Also, the resulting power deviation is 0.01–1.15% of the MPP power produced for ΔT = 40.3 °C.

The experimentally measured current–voltage curves of two TEG modules connected in parallel, for several temperature gradients, are presented in Fig. 9(a). For tracking the MPP, the control unit of the proposed system was configured to operate with a value of $R_{TEG,c} = 25.7/2 = 12.85\ \Omega$ in (8). The corresponding experimental power–voltage curves of two TEG modules connected in parallel, as well as the actual MPPs and the operating points detected as MPPs by the proposed MPPT system, are shown in Fig. 9(b). As shown in Fig. 10, the percentage deviation (i.e. tracking accuracy) is in the range of 0.01–1.46% for 20.4–40 °C temperature gradients, while it is increased up to 34.43% for lower values of ΔT. The power deviation is 0.01–2.41% of the MPP power produced for ΔT = 40.0 °C.

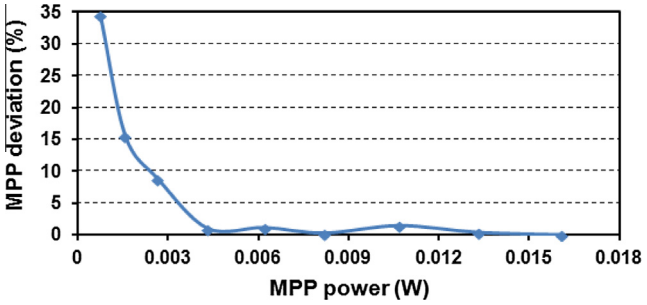

Fig. 10. The percentage deviation between the actual MPP of the power–voltage curve of a TEG array consisting of two TEG modules connected in parallel and the operating points detected by the proposed system as MPPs, for various values of ΔT.

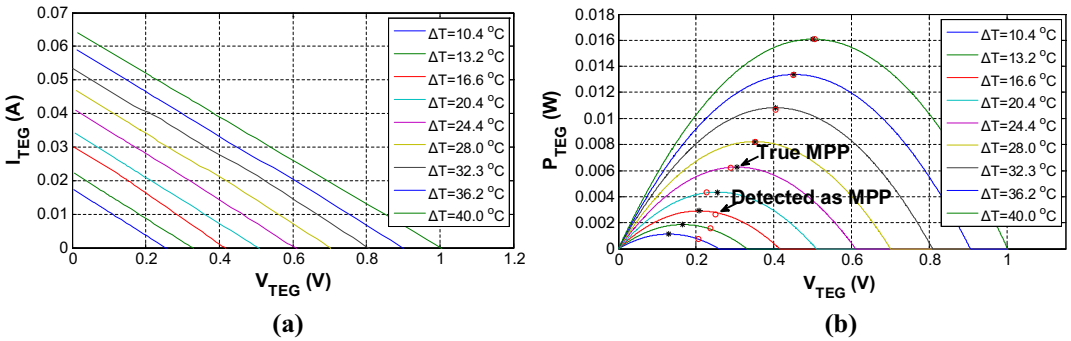

Fig. 9. Experimental characteristics for two TEG modules connected in parallel: (a) current–voltage and (b) power–voltage.

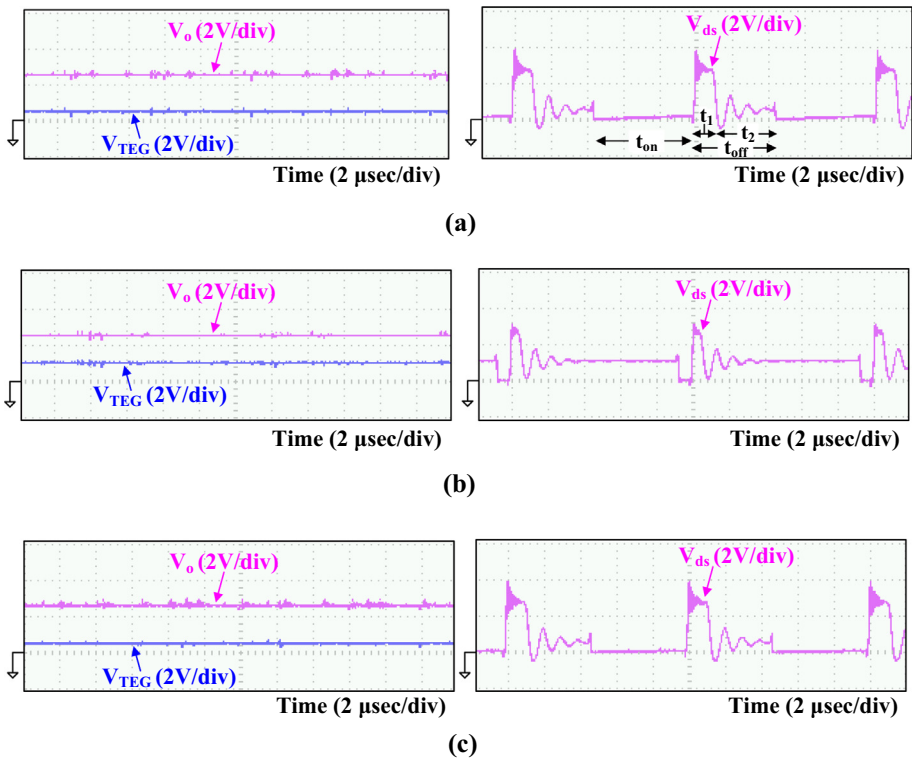

Fig. 11. Experimental waveforms of V_{TEG}, V_o and V_{ds} with ΔT = 40.0 °C for: (a) one TEG device, (b) two TEG modules connected in series and (c) two TEG modules connected in parallel.

In the experimental results presented in Figs. 5, 7 and 9, the deviation of the MPPs derived by the proposed system from the actual MPPs of the TEG source (i.e. tracking accuracy) is due to: (i) the non-ideal operation of the proposed control unit (especially at low DC input voltage and power levels for low values of ΔT) because of e.g. tolerance of circuit component values, circuit parasitics etc.; and (ii) the setting of $R_{TEG,c}$ in (8) to a constant value, without considering the effect of temperature, as analyzed in Section 3. However, the experimental results presented in Figs. 6, 8 and 10, reveal that the average (arithmetic mean) deviation of the power produced by the proposed system from the MPP power of the TEG source in the range of 1–17 mW, is 1.87%. Thus, the performance of the proposed MPPT system in terms of tracking accuracy, is comparable to the 95–99.85% MPP tracking efficiencies of the FOCV, P&O and InC methods [25], but it has been achieved using a simpler control system.

Experimental waveforms of V_{TEG}, V_o and V_{ds} of the Boost-type DC/DC converter (Fig. 4) with ΔT = 40.0 °C for one TEG device, two TEG modules connected in series and two TEG modules connected in parallel, respectively, are illustrated in Fig. 11. It is observed that in all cases, the DC output voltage of the DC/DC converter, V_o, is higher than the corresponding DC input voltage, V_{TEG}. During time interval t_{on}, which is indicated in Fig. 11(a), the power MOSFET of the DC/DC converter [i.e. S_m in Fig. 4(a)] is in the ON state, resulting in a zero V_{ds} voltage. Then, during time interval t_{off} the power MOSFET is turned-off. Since the DC/DC converter operates in the DCM, the drain-source voltage V_{ds} rises up to V_o during subinterval t_1 of t_{off}, where the current of the DC/DC converter inductor [i.e. L in Fig. 4(a)] is non-zero, due to the conduction of the DC/DC converter diode (i.e. D_s in Fig. 4). During time interval t_2, the inductor current has been dropped to zero, thus V_{ds} is clamped to the DC input voltage level, V_{TEG}. A similar response is also observed in the waveforms depicted in Fig. 11(b) and (c), respectively. The high-frequency ringing exhibited by V_{ds} is due to the inductive and capacitive parasitic components of the power converter devices and circuit board. As validated by the experimental results presented above, this high-frequency ringing does not affect the operation of the proposed MPPT system due to the use of a low-pass filter [see Fig. 4(a)] for measuring the value of I_{TEG}, as analyzed in Section 3. However, it can be suppressed through the connection of a suitable RC snubber across the drain and source terminals of the power MOSFET, in order to reduce the switching power losses of the power converter semiconductor devices [22].

An example of the signal S waveform, as well as the output of the PI controller [see Fig. 4(a)] during operation of the proposed MPPT system, is shown in Fig. 12. The operational amplifiers employed in the experimental prototype of the proposed control unit are power-supplied by the battery bank (total nominal voltage of $V_o = 2.4$ V), which is connected at the output of the power converter. Thus, the corresponding circuits have been tuned such that the signals S and "0 V" in Fig. 4(a) exhibit a DC offset of $V_o/2 = 1.2$ V with respect to the negative terminal of the battery bank, which corresponds to the ground levels indicated in Figs. 4 (a) and 12, respectively. Through this approach, the output of the PI controller and signal S may take either zero, positive or negative values with respect to "0 V". This is indispensable for identifying the position of each operating point on the power–voltage curve of the TEG source and, subsequently, forcing the control loop to converge to the MPP where (8) is satisfied, as discussed in Section 3.

The power consumption of the proof-of-principle experimental prototype of the proposed MPPT control unit has been measured to be equal to 5.13 mW. Due to the structure of the proposed control unit, this power consumption is independent of the TEG source power rating and remains constant for higher values of the TEG source power level. The developed laboratory prototype system is suitable for use in applications where the total power produced

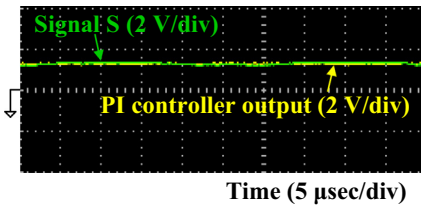

Fig. 12. An example of the signal *S* waveform, as well as the output of the PI controller during operation of the proposed MPPT system.

by the TEGs is higher than the power consumption of the control system. However, in this paper, the operation of the proposed MPPT system has also been investigated for DC input power levels below 5.13 mW, as described above, for exploring the performance of the proposed MPPT method at low power levels. Based on the information provided in the datasheets of the integrated circuits, which have been employed to build the control unit, it is estimated that approximately half of the 5.13 mW control unit power dissipation is consumed by the three AD8515 operational amplifiers comprising the PWM generator. The experimental prototype of the proposed MPPT control unit has been built for performance evaluation purposes, using discrete parts of commercially-available integrated circuits, which enables rapid prototyping with relatively low cost. However, similarly to the development process employed in [12], the proposed control unit can also be implemented in the form of an integrated circuit using CMOS technology for reducing its power consumption to the μW level. This will also enable its application in low-power (e.g. hundreds of μW) thermoelectric energy harvesting systems (e.g. [23]). In such a case, different alternative microelectronic circuits may be used to implement the functional elements of the proposed MPPT control system (i.e. amplifiers, PWM generator etc.), which are illustrated in Fig. 4(a).

5. Comparison with the past-proposed MPPT methods for TEGs

The control circuit elements required to implement the prior-art MPPT methods for TEG sources (see Section 1), as well as the technique proposed in this paper, are presented in Table 1. In all MPPT methods, a PWM or square-wave generator must be used for controlling the power converter. Increasing the PWM frequency (i.e. switching frequency) enables to reduce the size of the power converter passive components and the associated power loss. However, the maximum switching frequency, which can be produced by microcontroller/DSPs with an on-chip PWM generator, is limited by their maximum permissible clock frequency. As an example, for generating the 100 kHz switching frequency of the experimental prototype of the proposed system with an 8-bit duty-cycle resolution (see Section 4), a microcontroller with a $2^8 \times 100$ kHz = 25.6 MHz clock frequency must be employed, which increases the power consumption of the control unit. Alternatively, an external PWM generation circuit may be interfaced to the microcontroller/DSP unit. Due to their algorithmic functionality, the implementation of the P&O, InC and single-sensor techniques is facilitated when using microcontroller/DSP devices, rather than discrete components (e.g. multiplier, registers, derivative calculator etc.), which would result in a highly complex circuit. The use of a microcontroller/DSP is mostly suitable for use in high-power TEG

Table 1
The operational characteristics of various MPPT methods for TEGs.

MPPT method	MPPT control unit elements	Disadvantages
P&O	Voltage & current sensors with signal-conditioning circuits, microcontroller with on-chip A/D converter and PWM generator	Steady-state oscillation around the MPP
InC	Voltage & current sensors with signal-conditioning circuits, microcontroller with on-chip A/D converter and PWM generator	Steady-state oscillation around the MPP
FOCV	Voltage sensor with signal-conditioning circuit and: – one additional switch for open-circuiting the TEG source, sample-and-hold unit, timer, voltage controller and PWM generator or – a microcontroller with on-chip A/D converter and PWM generator Two temperature sensors with signal-conditioning circuits	Power loss during measurement of $V_{TEG,oc}$ High cost
FSCC	Current sensor with signal-conditioning circuit and: – one additional switch for short-circuiting the TEG source, sample-and-hold unit, timer, current controller, PWM generator or – a microcontroller with on-chip A/D converter and PWM generator	Power loss during measurement of $I_{TEG,sc}$
Single-sensor MPPT	Current sensor with signal-conditioning circuit, DSP with on-chip A/D converter and PWM generator	Complexity due to operation based on a model of the power converter
ImpM	– Two input/output voltage sensors with signal-conditioning circuits and a microcontroller with on-chip A/D converter and PWM generator or – Square-wave generator with adjustable duty cycle and frequency	– Requires knowledge of the power converter inductance – Accuracy affected by tolerance of inductance value – Less flexibility of selecting the inductance and switching frequency for achieving optimal efficiency and cost – Requires operation in DCM, which is not desirable at high power levels – DCM requires power semiconductors of a high current-rating
ESC	Voltage & current sensors with signal-conditioning circuits and: – high-pass filter, multiplier, sine-wave generator, integrator, adder, PWM generator or – microcontroller with on-chip A/D converter and PWM generator	Requires tuning of multiple parameters
Proposed method	– RC-based low-pass filter, – Operational-amplifier-based circuits: one IA, one voltage-follower, two adders and a PI controller, – PWM generator	Theoretically, less than 1.1% mismatch between the TEG MPPs and the actual operating points in the temperature range of $\Delta T = 1 - 100\ ^\circ C$

systems, where additional functions (e.g. battery-bank charging regulation, state of charge estimation etc.) are also incorporated in the algorithm executed by the microcontroller/DSP device.

In the FOCV, FSCC and single-sensor methods, one sensor must be employed for executing the MPPT control process, together with the accompanying signal-conditioning circuits, while the rest MPPT techniques require two sets of sensors and signal-conditioning circuits. However, the hardware resources employed for implementing the FOCV and FSCC MPPT methods are relatively high. This is due to the requirement of specialized circuits which must be employed, such as a sample-and-hold unit, which is controlled by a timer, for storing the TEG open-circuit voltage or short-circuit current until the next sampling cycle. Then, a voltage/current controller, which typically comprises a PI control module, adjusts the power converter duty cycle such that the TEG output voltage or current, respectively, is regulated to the desired value. Also, depending on the power converter topology, a power switch together with the corresponding gate-drive circuit may have to be added in the power converter circuit for open-/short-circuiting the TEG source. This increases the cost of the power-processing circuit proportionally to the power rating of the TEG energy-conversion system. The FOCV MPPT method implementation employing two temperature sensors, also results in a relatively high system cost, especially in case that the TEG source operating temperature range is high (e.g. in combustion engine applications).

The control unit complexity in the single-sensor MPPT method is relatively high due to the need of using a DSP unit in order to perform the calculations required by the power converter model during the MPPT process. Thus, the application of this method in low-power energy harvesting applications is not feasible due to the resulting high power-consumption of the control unit. The ImpM technique can easily be implemented either using discrete components, or within an IC, but exhibits significant operational disadvantages (see Section 1 and Table 1). The hardware complexity of the ESC MPPT method is relatively higher due to the need of more specialized circuits for its application. This complexity is further enhanced by the requirement of having the ability to tune multiple parameters in order to achieve a successful operation.

In contrast to the past-proposed MPPT methods for TEGs, the design of the proposed MPPT control system (i.e. Fig. 4) is based on only a few ordinary micro-power operational amplifiers, as analyzed in Section 3, which are relatively simple to either use as discrete components, or built within an IC. The control technique presented in this paper is simpler in terms of implementation, since it is not required to include an additional power switch, or use specialized and/or power-consuming circuit elements. Also, it is not constrained by the maximum PWM frequency generation capability of microcontroller/DSP devices and does not require either knowledge of the power converter inductance, or tuning of multiple parameters. Simultaneously, as analyzed in Section 4, the proposed technique achieves a tracking accuracy which is comparable with that of the FOCV, P&O and InC methods.

6. Conclusions

Thermoelectric generators are employed for harvesting the ambient thermal energy in order to power-supply a wide variety of devices, such as sensors, actuators and medical devices, in the μW up to several hundreds of Watts range. The power–voltage characteristic of a TEG array exhibits a unique MPP where the power produced by the TEG source is maximized. The MPP position changes according to the temperature gradient, which is developed across the surfaces of the individual TEG elements comprising the TEG source.

In this paper, an MPPT method for TEGs has been presented, which is suitable for application in both low- and high-power energy harvesting applications. The proposed technique is based on controlling a power converter such that it operates on a preprogrammed locus of operating points, which are located close to the MPPs of the power–voltage curve of the TEG power source. In contrast to the past-proposed MPPT methods for TEGs, the design of the proposed MPPT control system is based on only a few ordinary micro-power operational amplifiers, which are relatively simple to either use as discrete components, or built within an IC. The control technique presented in this paper is simpler in terms of implementation, since it is not required to include an additional power switch, or use specialized and/or power-consuming circuit elements characterized by a high development cost. Also, it is not constrained by the maximum PWM frequency generation capability of microcontroller/DSP devices and does not require either knowledge of the power converter inductance, or tuning of multiple parameters. Simultaneously, the proposed technique achieves a tracking accuracy which is comparable with that of the FOCV, P&O and InC methods.

References

[1] Park J-D, Lee H, Bond M. Uninterrupted thermoelectric energy harvesting using temperature-sensor-based maximum power point tracking system. Energy Convers Manage 2014;86:233–40.
[2] Yu Shuhai, Du Qing, Diao Hai, Shu Gequn, Jiao Kui. Effect of vehicle driving conditions on the performance of thermoelectric generator. Energy Convers Manage 2015;96:363–76.
[3] Du Qing, Diao Hai, Niu Zhiqiang, Zhang Guobin, Shu Gequn, Jiao Kui. Effect of cooling design on the characteristics and performance of thermoelectric generator used for internal combustion engine. Energy Convers Manage 2015;101:9–18.
[4] Shi Yongming, Wang Yao, Deng Yuan, Gao Hongli, Lin Zhen, Zhu Wei, et al. A novel self-powered wireless temperature sensor based on thermoelectric generators. Energy Convers Manage 2014;80:110–6.
[5] Lossec M, Multon B, Ahmed HB. Sizing optimization of a thermoelectric generator set with heatsink for harvesting human body heat. Energy Convers Manage April 2013;68:260–5.
[6] Bonin R, Boero D, Chiaberge M, Tonoli A. Design and characterization of small thermoelectric generators for environmental monitoring devices. Energy Convers Manage 2013;73:340–9.
[7] Yadav S, Yamasani P, Kumar S. Experimental studies on a micro power generator using thermoelectric modules mounted on a micro-combustor. Energy Convers Manage 2015;99:1–7.
[8] Barma MC, Riaz M, Saidur R, Long BD. Estimation of thermoelectric power generation by recovering waste heat from biomass fired thermal oil heater. Energy Convers Manage 2015;98:303–13.
[9] Kim S, Chou PH. Size and topology optimization for supercapacitor-based sub-Watt energy harvesters. IEEE Trans Power Electron 2013;28(4):2068–80.
[10] Mamur H, Ahiska R. Application of a DC–DC boost converter with maximum power point tracking for low power thermoelectric generators. Energy Convers Manage 2015;97:265–72.
[11] Laird I, Lu DDC. Steady state reliability of maximum power point tracking algorithms used with a thermoelectric generator. In: 2013 IEEE international symposium on circuits and systems (ISCAS); 2013. p. 1316–19.
[12] Huang C-J, Chen W-C, Ni C-L, Chen K-H, Lu C-C, Chu Y-H, et al. Thermoelectric energy harvesting with 1 mV low input voltage and 390 nA quiescent current for 99.6% maximum power point tracking. In: 2012 proceedings of the ESSCIRC (ESSCIRC); 2012. p. 105–108.
[13] Im J-P, Wang S-W, Ryu S-T, Cho G-H. A 40 mV transformer-reuse self-startup boost converter with MPPT control for thermoelectric energy harvesting. IEEE J Solid-State Circuits 2012;47(12):3055–67.
[14] Kim J, Kim C. A DC–DC boost converter with variation-tolerant MPPT technique and efficient ZCS circuit for thermoelectric energy harvesting applications. IEEE Trans Power Electron 2013;28(8):3827–33.
[15] Laird I, Lu DDC. High step-up DC/DC topology and MPPT algorithm for use with a thermoelectric generator. IEEE Trans Power Electron 2013;28(7):3147–57.
[16] Yamada H, Kimura K, Hanamoto T, Ishiyama T, Sakaguchi T, Takahashi T. A MPPT control method of thermoelectric power generation with single sensor. In: 2013 IEEE 10th international conference on power electronics and drive systems (PEDS); 2013. p. 936–41.
[17] Bandyopadhyay S, Chandrakasan AP. Platform architecture for solar, thermal, and vibration energy combining with MPPT and single inductor. IEEE J Solid-State Circuits 2012;47(9):2199–215.
[18] Ramadass YK, Chandrakasan AP. A battery-less thermoelectric energy harvesting interface circuit with 35 mV startup voltage. IEEE J Solid-State Circuits 2011;46(1):333–41.

[19] Phillip N, Maganga O, Burnham KJ, Ellis MA, Robinson S, Dunn J, et al. Investigation of maximum power point tracking for thermoelectric generators. J Electron Mater 2013;42(7):1900–6.
[20] Brownell E, Hodes M. Optimal design of thermoelectric generators embedded in a thermal resistance network. IEEE Trans Compon, Packaging Manuf Technol 2014;4(4):612–21.
[21] Dalola S, Ferrari M, Ferrari V, Guizzetti M, Marioli D, Taroni A. Characterization of thermoelectric modules for powering autonomous sensors. IEEE Trans Instrum Meas 2009;58(1):99–107.
[22] Mohan N, Undeland TM, Robbins WP. Power electronics: converters, applications, and design. 3rd ed. New York, NY, USA: Wiley; 2002.
[23] Weng P-S, Tang H-Y, Ku P-C, Lu L-H. 50 mV-input batteryless boost converter for thermal energy harvesting. IEEE J Solid-State Circuits 2013;48(4):1031–41.
[24] Mo C, Davidson J. Energy harvesting technologies for structural health monitoring applications. In: 2013 1st IEEE conference on technologies for sustainability (SusTech); 2013. p. 192–98.
[25] Montecucco A, Knox AR. Maximum power point tracking converter based on the open-circuit voltage method for thermoelectric generators. IEEE Trans Power Electron 2015;30(2):828–39.